PHYSICAL REVIEW B **87**, 100402(R) (2013)

Skyrmion dynamics in multiferroic insulators

Ye-Hua Liu,[1] You-Quan Li,[1] and Jung Hoon Han[2,3,*]

[1]*Zhejiang Institute of Modern Physics and Department of Physics, Zhejiang University, Hangzhou 310027, People's Republic of China*

[2]*Department of Physics and BK21 Physics Research Division, Sungkyunkwan University, Suwon 440-746, Korea*

[3]*Asia Pacific Center for Theoretical Physics, Pohang, Gyeongbuk 790-784, Korea*

(Received 14 September 2012; revised manuscript received 19 November 2012; published 13 March 2013)

The recent discovery of a Skyrmion crystal phase in an insulating multiferroic compound Cu_2OSeO_3 calls for new ways and ideas to manipulate the Skyrmions in the absence of spin transfer torque from the conduction electrons. It is shown here that the position-dependent electric field, pointed along the direction of the average induced dipole moment of the Skyrmion, can induce the Hall motion of the Skyrmion with its velocity orthogonal to the field gradient. Finite Gilbert damping produces longitudinal motion. Inter-Skyrmion interaction leads to the reduction of the drift speed. We find a rich variety of resonance modes excited by an ac electric field.

DOI: 10.1103/PhysRevB.87.100402 PACS number(s): 75.85.+t, 75.70.Kw, 76.50.+g

Skyrmions are fast becoming common sightings among spiral magnets including many of the metallic B20 compounds[1–5] and most recently, in a multiferroic insulator Cu_2OSeO_3.[6] Both species of compounds display similar thickness-dependent phase diagrams[5,6] despite their completely different electrical properties, highlighting the generality of the Skyrmion phase in spiral magnets. Along with the ubiquity of Skyrmion matter comes the challenge of finding a means to control and manipulate them, in a device-oriented manner akin to efforts in the spintronics community to control the domain wall and vortex motion by electrical current. Spin transfer torque (STT) is a powerful means to induce fast domain-wall motion in metallic magnets.[7,8] Indeed, current-driven Skyrmion rotation[9] and collective drift,[10] originating from STT, have been demonstrated recently. Theory of current-induced Skyrmion dynamics has been worked out in Refs. 11–13. In insulating compounds such as Cu_2OSeO_3, however, the STT-driven mechanism does not work due to the lack of conduction electrons.

Spiral magnetic order in Cu_2OSeO_3 is accompanied by a finite electric dipole moment as experimentally demonstrated by Seki *et al.*[14] due to the *pd*-hybridization mechanism.[14–18] In short, a given magnetization $\mathbf{S}_i$ induces electric dipole moment $\mathbf{P}_i$ with the relation

$$\mathbf{P}_i = \lambda\left(S_i^y S_i^z, S_i^z S_i^x, S_i^x S_i^y\right) \tag{1}$$

through some coupling λ. Each site i corresponds to one cubic unit cell of Cu_2OSeO_3 with linear dimension $a \sim 8.9$ Å, and we have normalized $\mathbf{S}_i$ to have unit magnitude. The dimension of the coupling constant is therefore $[\lambda] = \mathrm{C\,m}$. Formula (1) was recently obtained for Cu_2OSeO_3 from the Ginzburg-Landau symmetry argument[18] and appeared in the earlier discussion of another *pd*-hybridization-induced multiferroic insulator, $Ba_2CoGe_2O_7$.[19,20] Although not explicitly mentioned in previous theories,[18,20] the same formula is applicable to the Skyrmion lattice phase as well. In Ref. 14 microscopic *pd* polarizations were added up numerically without relying on formula (1) to deduce the dipole moment of the Skyrmion. We have verified, as shown in Fig. 1, that insertion of the Skyrmion spin configuration $\mathbf{S}_i$ in Eq. (1) yields the electric dipole moment distribution that agrees very well with the numerically obtained profile shown in Fig. 4 of Ref. 14. Taking this agreement a step further, we use Eq. (1) to demonstrate that an electric-field gradient can induce Skyrmion motion by coupling efficiently to the Skyrmion's dipole moment. The proposed mechanism may provide a solid means for manipulating insulating Skyrmions and is complementary to the current-driven mechanism[12] that works on metallic Skyrmions.

Equation (1) implies the presence of the magnetoelectric coupling Hamiltonian

$$H_{\mathrm{ME}} = -\sum_i \mathbf{P}_i \cdot \mathbf{E}_i = -\lambda \sum_i \left(E_i^x S_i^y S_i^z + \text{cyclic perm.}\right), \tag{2}$$

in addition to the Heisenberg and Dzyaloshinskii-Moriya exchange interactions among spins (H_{HDM}) and the Zeeman interaction with the external magnetic field $H_{\mathrm{Z}} = -\mathbf{B} \cdot \sum_i \mathbf{S}_i$ in Cu_2OSeO_3. Earlier theoretical studies established that $H_{\mathrm{HDM}} + H_{\mathrm{Z}}$ can stabilize the Skyrmion phase under a moderate magnetic field.[1,21–24] The magnetoelectric Hamiltonian H_{ME} in essence provides the spin anisotropy by application of the electric field. The Landau-Lifshitz-Gilbert (LLG) equation corresponding to $H = H_{\mathrm{HDM}} + H_{\mathrm{Z}} + H_{\mathrm{ME}}$ can be readily derived as $\dot{\mathbf{S}}_i + (1/\hbar)\mathbf{S}_i \times (\delta H/\delta \mathbf{S}_i) + \alpha \mathbf{S}_i \times \dot{\mathbf{S}}_i = 0$ and solved by numerical integration for some Gilbert damping constant α.

In the experiment of Ref. 14, three crystallographically distinct orientations were chosen for measuring the magnetic-field-induced polarization. Categorizing the experimental findings, the magnetic field and induced Skyrmion dipole moment orientations are, respectively, (I) $\mathbf{B}\|[001]$, $\mathbf{P} = 0$, (II) $\mathbf{B}\|[110]$, $\mathbf{P}\|[001]$, and (III) $\mathbf{B}\|[111]$, $\mathbf{P}\|[111]$. In case (I) only a net quadrupole moment is induced on the Skyrmion. In cases (II) and (III) an electric field can be imposed parallel to the dipole moment, $\mathbf{E}_i = E_i \hat{\mathbf{P}}$ ($\hat{\mathbf{P}} = \mathbf{P}/|\mathbf{P}|$), to maximize the magnetoelectric coupling and enhance the electric field control. To simplify the subsequent calculation we choose to make an orthogonal rotation $\mathcal{R}$ of the spin axis $\mathbf{S}_i \to \mathcal{R}\mathbf{S}_i'$ appearing in Eq. (1) so that the z direction of the new spin $\mathbf{S}_i'$ coincides with the $\mathbf{B}$-field orientation in a given setup and its x direction with the crystallographic $[\bar{1}10]$ since it is orthogonal to all three $\mathbf{B}$-field directions used in the experiment. In each of the cases listed above we obtain the magnetoelectric coupling,

 ©2013 American Physical Society

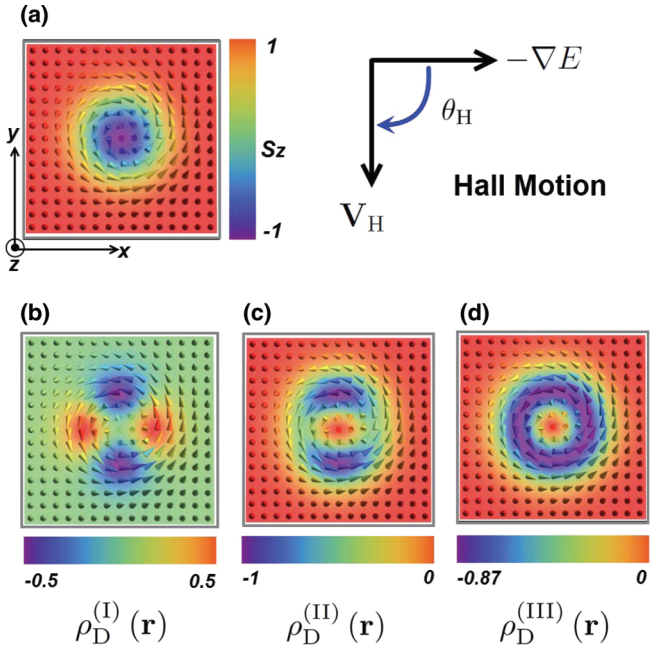

FIG. 1. (Color online) (a) Typical Skyrmion configuration and (b)–(d) the corresponding distribution of dipole density $\rho_D(\mathbf{r})$ for three magnetic field orientations used in Ref. 14. For precise definition of $\rho_D(\mathbf{r})$ used, see the Supplemental Material (Ref. 25). (b) $\mathbf{B}\|[001]$. (c) $\mathbf{B}\|[110]$. (d) $\mathbf{B}\|[111]$. As schematically depicted in (a), the Skyrmion executes a Hall motion in response to the electric field gradient.

expressed in the respective rotated spin frames,

$$H_{\rm ME}^{(\rm I)} = -(\lambda/2)\sum_i E_i\left(\left[S_i^y\right]^2 - \left[S_i^x\right]^2\right),$$
$$H_{\rm ME}^{(\rm II)} = -(\lambda/2)\sum_i E_i\left(\left[S_i^z\right]^2 - \left[S_i^x\right]^2\right), \quad (3)$$
$$H_{\rm ME}^{(\rm III)} = -(\lambda/2\sqrt{3})\sum_i E_i\left(3\left[S_i^z\right]^2 - 1\right).$$

Primes have been dropped from $\mathbf{S}_i'$ in the above expressions. In case (I) where there is no net dipole moment for Skyrmions we chose $\mathbf{E}\|[001]$ to arrive at a simple magnetoelectric coupling form shown above. In cases (II) and (III) $\mathbf{E}$-field direction coincides with that of the dipole moment.

Suppose now that the $\mathbf{E}$-field variation is sufficiently slow on the scale of the lattice constant a to allow the rewriting of $H_{\rm ME}$ in Eq. (3) in the continuum as $H_{\rm ME} = -\lambda(d/a)\int d^2\mathbf{r}\; E(\mathbf{r})\rho_D(\mathbf{r})$. It will be assumed that all variables behave identically along the thickness direction, of length d. The dipole density $\rho_D(\mathbf{r})$, shown in Figs. 1(b)–1(d) for cases (I)–(III), couples to the electric field $E(\mathbf{r})$ in the same way as the conventional electric charge density does to the potential field in electromagnetism. The analogy will be useful when we think about the Skyrmion dynamics under the spatially varying $\mathbf{E}$ field. As in Ref. 12 we view the individual Skyrmion as a pointlike object described by the distribution $\rho_D(\mathbf{r}) = Q_D N_{\rm Sk}\sum_j \delta(\mathbf{r}-\mathbf{r}_j)$, where $\mathbf{r}_j$ spans the Skyrmion positions and identical dipole charge Q_D is assumed for all the Skyrmions. Explicit definitions of $\rho_D(\mathbf{r})$ and Q_D appear in the Supplemental Material,[25] while $N_{\rm Sk}$ is the number of spins inside a Skyrmion. The magnetoelectric coupling energy is transformed to the "potential energy" of the collection of Skyrmion particles,

$$H_{\rm ME} = -\lambda Q_D N_{\rm Sk}\frac{d}{a}\sum_j E(\mathbf{r}_j). \quad (4)$$

A force acting on the Skyrmion will be $\mathbf{F}_i = -\nabla_i H_{\rm ME}$. Inter-Skyrmion interaction is ignored.

The response of Skyrmions to a given force is that of an electric charge in a strong magnetic field, embodied in the Berry phase action $(-2\pi S\hbar Q_{\rm Sk} d/a^3)\sum_j \int dt(\mathbf{r}_j\times\dot{\mathbf{r}}_j)\cdot\hat{z}$, where $Q_{\rm Sk}$ is the quantized Skyrmion charge[12,26] and S is the size of spin. An equation of motion follows from the combination of the Berry phase action and Eq. (4):

$$\mathbf{v}_j = \frac{\lambda l_{\rm Sk}^2}{4\pi S\hbar}\frac{Q_D}{Q_{\rm Sk}}\hat{z}\times\nabla_j E(\mathbf{r}_j), \quad (5)$$

where $\mathbf{v}_j$ is the jth Skyrmion velocity and $l_{\rm Sk}^2 \equiv N_{\rm Sk}a^2$. Typical speed of the Hall motion can be estimated by replacing $|\lambda\nabla E|$ with $\Delta\mathcal{E}_{\rm dipole}/l_{\rm Sk}$, where $\Delta\mathcal{E}_{\rm dipole}$ is the difference in the dipolar energy felt at the left and the right edges of the Skyrmion and $l_{\rm Sk}$ is its diameter. This way one arrives at the speed of the Hall motion

$$v_H \sim \frac{1}{4\pi S}\frac{Q_D}{Q_{\rm Sk}}\frac{l_{\rm Sk}}{t_{\rm Sk}}, \quad t_{\rm Sk} = \frac{\hbar}{\Delta\mathcal{E}_{\rm dipole}}, \quad (6)$$

written, apart from numerical factors, as the linear dimension of the Skyrmion divided by the "Skyrmion time" $t_{\rm Sk}$ as decided by the dipolar energy difference applied across its length. Adopting experimental input parameters of $l_{\rm Sk} = 10^{-7}$ m, and $\lambda = 10^{-32}$ C m from Ref. 14 and using $Q_D = -1$ and $Q_{\rm Sk} = -1$, we find the velocity $v_H \sim 10^{-6}\Delta E[\mathrm{m^2/V\,s}]$, which gives the estimated drift velocity of 1 mm/s for the field strength difference $\Delta E = 10^3$ V/m across the Skyrmion. We may as well estimate the maximum allowed drift velocity by equating the dipolar energy difference $\Delta\mathcal{E}_{\rm dipole}$ across the Skyrmion to the exchange energy J, also corresponding to the formation energy of one Skyrmion.[24] The maximum expected velocity thus obtained is enormous, $\sim 10^4$m/s for $J \sim 1$ meV, implying that with the right engineering one can achieve rather high Hall velocity of the Skyrmion. In an encouraging step forward, electric-field control of the Skyrmion lattice orientation in the Cu_2OSeO_3 crystal was recently demonstrated.[27]

Results of LLG simulation are discussed next. To start, a linear field configuration $E_{i_x,i_y} = ai_x + b$ is imposed on a rectangular simulation lattice $1 \leqslant i_x \leqslant L_x$, $1 \leqslant i_y \leqslant L_y$, with both L_x and L_y much larger than the Skyrmion size. In the absence of Gilbert damping, a single Skyrmion placed in such an environment moved along the "equipotential line" in the y direction as expected from the guiding-center dynamics of Eq. (5). In cases (II) and (III) the dipole charges obey the relation $Q_D^{(\rm II)}/Q_D^{(\rm III)} = \sqrt{3}/2$ as discussed in the Supplemental Material,[25] and based on Eq. (5) one would expect their respective drift velocities to scale with the same ratio. This is indeed the case as one can see in Fig. 2. Additionally, the numerical result of Hall velocity shows excellent agreement with that calculated by Eq. (5), which is $-0.0161v_0$ for case (II) and $-0.0192v_0$ for case (III). [Here we have defined $t_0 = (S\hbar)/(\lambda a)$ m^2/V and $v_0 = a/t_0$. For more details, see

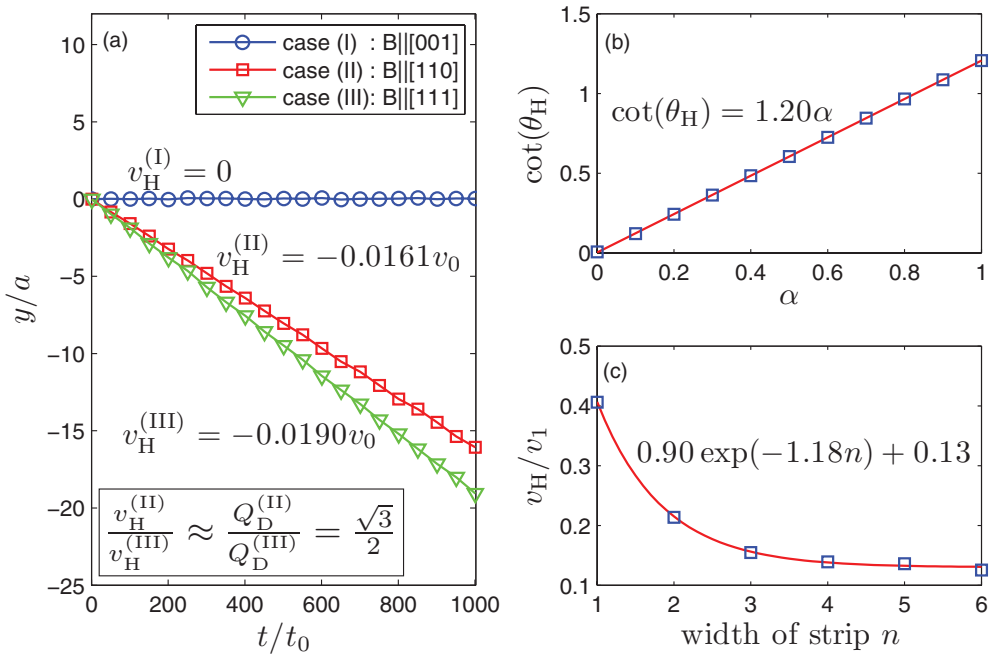

FIG. 2. (Color online) (a) Skyrmion position versus time for cases (I)–(III) for linear electric field modulation (see text) with the Skyrmion center placed at the center of the simulation lattice. The average Hall velocities in cases (II) and (III) indicated in the figure are approximately proportional to the respective dipolar charges, in agreement with Eq. (5). (b) Hall angle θ_H vs Gilbert damping parameter α. (c) Hall motion speed v_H vs number of Skyrmion layers n in the strip. Unit of the speed v_1 is for the single Skyrmion subject to the same field gradient.

the Supplemental Material.[25]] The drift velocity decreased continuously as we reduced the field gradient, obeying the relation (5) down to the zero velocity limit. The dipolar charge is zero in case (I), and indeed the Skyrmion remains stationary for the linear field gradient as shown in Fig. 2(a). If the field variation is sufficiently rapid, however, the forces acting on the positive dipole density blobs [red in Fig. 1(a)] may not be completely canceled by those on the negative dipole density blobs [blue in Fig. 1(a)] permitting some Skyrmion drift motion.

Longitudinal motion along the field gradient begins to develop with finite Gilbert damping, driving the Skyrmion center to the position of lower potential energy $E(\mathbf{r})$. As a result, the trajectory of Skyrmion in response to the uniform field gradient is still linear but deviates from the perfect Hall angle $\theta_H = \pi/2$. By doing a series of simulations in linear profile of the $\mathbf{E}$ field with different damping parameters α we observed the Hall angle obeying the relation $\cot\theta_H = 1.20\alpha$ as shown in Fig. 2(b), in good agreement with the prediction of Ref. 12 provided the so-called shape factor chosen is $\eta = 1.2$.

For the Skyrmion lattice case, imposing a uniform field gradient across the whole lattice may be too demanding experimentally, unless the magnetic crystal is cut in the form of a narrow strip the width of which is comparable to a few Skyrmion radii. With this situation in mind we calculated the collective drift velocity of the Skyrmion lattice with n columns of Skyrmions in the strip subject to the uniform field gradient in the direction of the row. The collective Hall drift velocity taking place along the column direction displayed in Fig. 2(c) shows the exponential decrease of the drift speed with the thickness n, reaching the saturated value of ~13% of the single Skyrmion Hall velocity, denoted as v_1 in Fig. 2(c), subject to the same field gradient. The interaction of a Skyrmion with other Skyrmions, as well as with the wall boundary, could be responsible for this reduction in the drift speed and, at the same time, excite some breathing modes of the individual Skyrmion as it drifts. These effects, however, deserve a separate careful study beyond the scope of this Rapid Communication.

Several movie files are included in the Supplemental Material. II.gif and III.gif give Skyrmion motion for $E_{i_x,i_y} = E_0 \sin(2\pi i_x/L_x)$ on the $L_x \times L_y = 66 \times 66$ lattice for magnetoelectric couplings (II) and (III) in Eq. (3). III-Gilbert.gif gives the same $\mathbf{E}$ field as III.gif, with finite Gilbert damping $\alpha = 0.2$. I.gif describes the case (I) where the average dipolar charge is zero, with a rapidly varying electric field $E_{i_x,i_y} = E_0 \sin(2\pi i_x/\lambda_x)$ and λ_x comparable to the Skyrmion radius. The case of a narrow strip with the field gradient across is shown in strip.gif.

Mochizuki's recent simulation[28] revealed that internal motion of Skyrmions can be excited with the uniform ac magnetic field. Some of his predictions were confirmed by the recent microwave measurement.[29] Here we show that a uniform ac *electric field* can also excite several internal modes due to the magnetoelectric coupling. A time-localized, uniform electric-field pulse $E_i(t) = Ee^{-t^2/(2\tau^2)}$, with some small constant E and τ much shorter than the typical vibration period of an excited mode, was applied in the LLG simulation and the temporal response of the Skyrmion lattice analyzed by measuring the response function $\chi_{(I)}(t) = (1/2)\sum_i([S_i^y(t)]^2 - [S_i^x(t)]^2)$, $\chi_{(II)}(t) = (1/2)\sum_i([S_i^z(t)]^2 - [S_i^x(t)]^2)$, and $\chi_{(III)}(t) = (\sqrt{3}/2)\sum_i[S_i^z(t)]^2$ for cases (I)–(III), respectively. In Mochizuki's work, the response function was the component of total spin along the ac magnetic field direction. For more details of the numerical procedure we

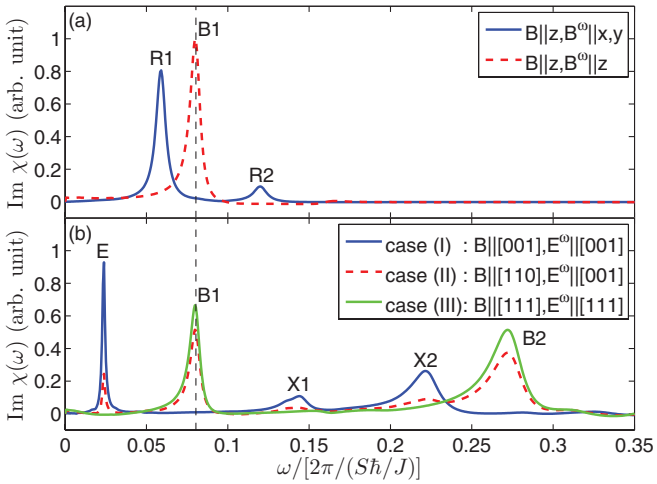

FIG. 3. (Color online) (a) Absorption spectra [imaginary part of the susceptibility] for an ac uniform magnetic field as in Mochizuki's work, reproduced here for comparison to an ac electric field response. (b) Absorption spectra for an ac uniform electric field in cases (I)–(III). In case (I) where there is no net dipolar charge we find three low-energy modes E, X1, and X2. For case (III) where the dipolar charge is finite we find B1 and B2 radial modes excited. Case (II) exhibits all five modes. A detailed description of each mode is given in the text.

refer to his paper.[28] Absorption spectra can be deduced by the Fourier transform $\chi(\omega) = (1/T)\int_0^T \chi(t)e^{i\omega t}\,dt$ over a sufficiently long simulation time T.

In case I, the uniform electric field perturbs the initial cylindrical symmetry of the Skyrmion spin profile so that $\sum_i([S_i^x(t)]^2 - [S_i^y(t)]^2)$ becomes nonzero and the overall shape becomes elliptical. The axes of the ellipse then rotates counterclockwise about the Skyrmion center of mass as illustrated in Supplemental Material figure E-mode.gif.[25] There are two additional modes of higher energies with broken cylindrical symmetry in case I, labeled X1 and X2 in Fig. 3 and included as X1-mode.gif and X2-mode.gif in the Supplemental Material.[25] The rotational direction of the X1 mode is the same as in the E mode, while it is the opposite for the X2 mode.

As in Ref. 28, we find sharply defined breathing modes in cases II and III at the appropriate resonance frequency ω; in fact the same frequency at which the ac magnetic field excites the breathing mode. The vertical dashed line in Fig. 3 indicates the common breathing mode frequency. Movie file B1-mode.gif shows the breathing mode in case III. The additional, higher energy B2 mode (B2-mode.gif) was found in cases II and III, which is the radial mode with one node, whereas the B1 mode is nodeless.

In addition to the two breathing modes, the E mode and the two X modes are excited in case (II) as well due to the partly in-plane nature of the spin perturbation $-(\lambda E(t)/2)\sum_i([S_i^z(t)]^2 - [S_i^x(t)]^2)$. In contrast, case (III), where the perturbation $-(\sqrt{3}\lambda E(t)/2)\sum_i[S_i^z(t)]^2$ is purely out of plane, one only finds the B modes. As a result, cases (I) and (III) have no common resonance modes or peaks, while case (II) has all the peaks (though the X1 and X2 peaks are small). Compared to the magnetic-field-induced resonances, a richer variety of modes are excited by the ac electric field. In particular, the E mode has lower excitation energy than the B mode and has a sharp resonance feature, which should make its detection a relatively straightforward task. Full analytic solution of the excited modes[30] will be given later.

In summary, motivated by the recent discovery of the magnetoelectric material Cu_2OSeO_3 exhibiting Skyrmion lattice phase, we have outlined the theory of Skyrmion dynamics in such materials. The electric field gradient is identified as the source of the Skyrmion Hall motion. Several resonant excitations by an ac electric field are identified.

J.H.H. is supported by NRF Grants No. 2010-0008529 and No. 2011-0015631. Y.Q.L. is supported by NSFC Grant No. 11074216. J.H.H. acknowledges earlier collaboration with N. Nagaosa, Youngbin Tchoe, and J. Zang on a related model and informative discussions with Y. Tokura.

*hanjh@skku.edu

[1] S. Mühlbauer, B. Binz, F. Jonietz, C. Pfleiderer, A. Rosch, A. Neubauer, R. Georgii, and P. Böni, Science **323**, 915 (2009).
[2] W. Münzer, A. Neubauer, T. Adams, S. Mühlbauer, C. Franz, F. Jonietz, R. Georgii, P. Böni, B. Pedersen, M. Schmidt, A. Rosch, and C. Pfleiderer, Phys. Rev. B **81**, 041203(R) (2010).
[3] X. Z. Yu, Y. Onose, N. Kanazawa, J. H. Park, J. H. Han, Y. Matsui, N. Nagaosa, and Y. Tokura, Nature (London) **465**, 901 (2010).
[4] X. Z. Yu, N. Kanazawa, Y. Onose, K. Kimoto, W. Z. Zhang, S. Ishiwata, Y. Matsui, and Y. Tokura, Nature Mater. **10**, 106 (2011).
[5] N. Kanazawa, Y. Onose, T. Arima, D. Okuyama, K. Ohoyama, S. Wakimoto, K. Kakurai, S. Ishiwata, and Y. Tokura, Phys. Rev. Lett. **106**, 156603 (2011).
[6] S. Seki, X. Z. Yu, S. Ishiwata, and Y. Tokura, Science **336**, 198 (2012).
[7] G. Tatara, H. Kohno, and J. Shibata, Phys. Rep. **468**, 213 (2008).
[8] D. C. Ralph and M. Stiles, J. Magn. Magn. Mater. **320**, 1190 (2008).
[9] F. Jonietz, S. Mühlbauer, C. Pfleiderer, A. Neubauer, W. Münzer, A. Bauer, T. Adams, R. Georgii, P. Böni, R. A. Duine, K. Everschor, M. Garst, and A. Rosch, Science **330**, 1648 (2010).
[10] T. Schulz, R. Ritz, A. Bauer, M. Halder, M. Wagner, C. Franz, C. Pfleiderer, K. Everschor, M. Garst, and A. Rosch, Nat. Phys. **8**, 301 (2012).
[11] K. Everschor, M. Garst, R. A. Duine, and A. Rosch, Phys. Rev. B **84**, 064401 (2011).
[12] J. Zang, M. Mostovoy, J. H. Han, and N. Nagaosa, Phys. Rev. Lett. **107**, 136804 (2011).
[13] Y. Tokura and S. Seki, Adv. Mater. **22**, 1554 (2010).
[14] S. Seki, S. Ishiwata, and Y. Tokura, Phys. Rev. B **86**, 060403(R) (2012).
[15] Chenglong Jia, Shigeki Onoda, Naoto Nagaosa, and Jung Hoon Han, Phys. Rev. B **74**, 224444 (2006).
[16] Chenglong Jia, Shigeki Onoda, Naoto Nagaosa, and Jung Hoon Han, Phys. Rev. B **76**, 144424 (2007).

[17]Taka-hisa Arima, J. Phys. Soc. Jpn. **76**, 073702 (2007).

[18]M. Belesi, I. Rousochatzakis, M. Abid, U. K. Rößler, H. Berger, and J.-Ph. Ansermet, Phys. Rev. B **85**, 224413 (2012).

[19]H. Murakawa, Y. Onose, S. Miyahara, N. Furukawa, and Y. Tokura, Phys. Rev. Lett. **105**, 137202 (2010).

[20]Judit Romhányi, Miklós Lajkó, and Karlo Penc, Phys. Rev. B **84**, 224419 (2011).

[21]A. N. Bogdanov and D. A. Yablonskii, Sov. Phys. JETP **68**, 101 (1989); A. Bogdanov and A. Hubert, J. Magn. Magn. Mater. **138**, 255 (1994).

[22]U. K. Roßler, A. N. Bogdanov, and C. Pfleiderer, Nature (London) **442**, 797 (2006).

[23]Su Do Yi, Shigeki Onoda, Naoto Nagaosa, and Jung Hoon Han, Phys. Rev. B **80**, 054416 (2009).

[24]Jung Hoon Han, Jiadong Zang, Zhihua Yang, Jin-Hong Park, and Naoto Nagaosa, Phys. Rev. B **82**, 094429 (2010).

[25]See Supplemental Material at http://link.aps.org/supplemental/10.1103/PhysRevB.87.100402 for details of numerical simulation.

[26]Michael Stone, Phys. Rev. B **53**, 16573 (1996).

[27]J. S. White, I. Levatić, A. A. Omrani, N. Egetenmeyer, K. Prša, I. Živković, J. L. Gavilano, J. Kohlbrecher, M. Bartkowiak, H. Berger, and H. M. Rønnow, J. Phys.: Condens. Matter **24**, 432201 (2012).

[28]Masahito Mochizuki, Phys. Rev. Lett. **108**, 017601 (2012).

[29]Y. Onose, Y. Okamura, S. Seki, S. Ishiwata, and Y. Tokura, Phys. Rev. Lett. **109**, 037603 (2012).

[30]Olga Petrova and Oleg Tchernyshyov, Phys. Rev. B **84**, 214433 (2011); Imam Makhfudz, Benjamin Krüger, and Oleg Tchernyshyov, Phys. Rev. Lett. **109**, 217201 (2012).